Link Characterization for Aerial Wireless Sensor Networks

Nadeem Ahmed Salil S. Kanhere Sanjay Jha

University of New South Wales, Australia
{nahmed,salilk, sanjay}@cse.unsw.edu.au

Technical Report
UNSW-CSE-TR-1113
August 2011

THE UNIVERSITY OF
NEW SOUTH WALES

School of Computer Science and Engineering
The University of New South Wales
Sydney 2052, Australia

Abstract

Characterization of communication links in Aerial Wireless Sensor Networks (AWSN) is of paramount importance for achieving acceptable network performance. Protocols based on an arbitrary link performance threshold may exhibit inconsistent behavior due to link behavior not considered during the design stage. It is thus necessary to account for factors that affect the link performance in real deployments. This report details observations from an extensive experimental campaign designed to characterize the behavior of communication links in AWSN. We employ the widely used TelosB sensor platform for these experiments. The experimental results highlight the fact that apart from the usual outdoor environmental factors affecting the link performance, two major contributors to the link degradation in AWSN are the antenna orientation and the multi-path fading effect due to ground reflections. Based on these observations, we recommend measures that can help alleviate the effect of these potential sources of performance degradation in AWSN in order to achieve acceptable network performance.

1 Introduction

Recent advances in embedded systems and robotics have enabled a new class of mobile sensor networks, which can significantly enhance the spatial coverage of the target region. Two main advantages of mobile sensors are that they can: (i) control the deployment, thus providing optimal coverage of the desired region and (ii) dynamically repair the network, thus eliminating transmission bottlenecks and effectively increasing the network efficiency. In recent years, mobile sensors have been successfully adopted for terrestrial [1] and ocean [2] monitoring. The next logical step in their evolution is to enable mobile sensors to explore the aerial dimension, i.e., design an airborne sensor network. The objective is to amalgamate the sensing and communicating capabilities of wireless sensor networks with the autonomous flying ability of micro aerial vehicles to engineer a novel paradigm, Multi-hop Aerial Wireless Sensor Network (AWSN), wherein these small aerial vehicles equipped with wireless radio and sensors sample the physical space in three dimensions and relay the data over the underlying multi-hop wireless network to ground stations. The ground stations may then forward the information to end users via the Internet. Aerial nodes can also complement ground-deployed sensors by providing unique three-dimensional vantage that would otherwise be infeasible. The low-cost fine-grain sensing capabilities of AWSN thus enable a variety of innovative applications spanning both the public and commercial domains: tracking bushfires, sensing toxic plume behavior, and disaster reconnaissance and recovery, for example.

The sensed data from the AWSN is relayed to a ground station by equipping the UAVs with a 802.11 or ZigBee transmitter. Given that the typical range of wireless technologies such as 802.11 and ZigBee is only a few meters, UAVs create a multi-hop aerial network such that the sensed information can be relayed back to a distant terrestrial base station. Network protocols are responsible for overseeing this data relay. In designing robust protocols, it is important to make realistic assumptions about the characteristics of the underlying communication links. This is particularly crucial in a dynamic aerial environment, since wireless communication can be affected by several factors such as interference, path loss, multi-path propagation and Doppler effect etc. It is therefore, necessary to derive realistic abstractions of the wireless communication properties for multi-hop AWSN. Recent research in AWSN has focused on distributed coordination for a swarm of UAVs [3], [4], coverage evaluation in 3D [5] etc. but not much work has been done on understanding the network connectivity dynamics for an AWSN.

A general consensus among the wireless research community is that simulation results alone do not adequately reflect the real behavior of wireless ad-hoc networks due to the simplified radio propagation models [6], [7], [8]. Protocols designed based solely on simulation studies do not always work when they are subjected to real deployments. This motivates the study of empirical link characterization in order to design robust and practical protocols for AWSN.

Most of the link characterization work for 3D wireless networks reported in the literature are either based on WiFi links [9], [10] or a combination of 802.11 and cellular communications [11], [12]. Authors in [13] reported results from an empirical study on RSSI variability in 3D ZigBee based network using mono-pole antennas. Their results showed that antenna orientation is a dominant factor affecting the RSSI sensitivity especially for 3D scenarios. Allred et.al. in [14] presented results from their ZigBee based wireless characterization experiments using XBee Pro mounted SensorFlock platform. The antenna used in the experiments was a quarter wave whip antenna that performed best when the transmit antenna orientation was close to 90 degrees. Teh et.al. [15] used the Fleck3 platform mounted on a fixed wing airborne vehicle to perform communication range testing. They employed an external antenna with the Fleck operating at 900 MHz band. Our work is different from the previous works in several ways. For our link characterization experiments, we employ widely used off-the-shelf TelosB platform [16], that has a PCB mounted inverted F antenna [17]. The use of off-the-shelf WSN devices permits easy integration with the UAV platform resulting in rapid design and deployment. We make the following specific contributions in this work:

- We empirically study the link behavior for better understanding of the wireless communication characteristics between nodes in an AWSN. Communication in AWSN takes place over 3 distinct kinds of links - (i) Ground-to-Air (G-A) typically used by base stations on the ground to relay configuration commands to UAVs (ii) Air-to-Air (A-A) used for inter UAV communication for forwarding data and movement coordination and (iii) Air-to-Ground (A-G) which are used for relaying sensor data from the UAVs to the base station. Intuitively, we expect that the performance of these three kinds of communication links in an AWSN would be different based on the transmitter-receiver antenna heights above ground and ground reflections etc. We characterize each type of link, both in isolation and in a multi-hop scenario, to evaluate the differences in their expected performance.

- We observe factors most critical for the design of robust network protocols in AWSN and make design recommendations that are generally applicable for any ZigBee based AWSN. The experimental results from a systematic set of link characterization experiments indicate that TelosB antennas have directional bias where the radiated signal strength varies in different directions. This affects the link quality based on the sender-receiver antenna. We also observed that fading effect due to ground reflections creates grey areas of communications where the link performance degrades considerably. A protocol designer must incorporate measures to alleviate the effect of these factors in order to achieve acceptable network performance.

Note that we have used static plastic poles for 3D placement of nodes for these link characterization experiments. The use of poles limits the height of the sender/receivers (4.2m is the maximum height used in the experiments) but gives more control over the test environment in conducting and repeating the topology experiments. Also, this static placement of the nodes does not capture the effect of UAV movements (e.g., the Doppler effect) on the link characteristics. We do not expect Doppler effect to be severe at the mobility speed of a few km/h typical for these hovering UAVs. The presented results are also specific to the TelosB WSN platform that we have utilized for our work. The antenna characteristics would be different for a WSN platform employing different antennas. We believe that the design recommendations from this study are still generally applicable for any low-powered ZigBee based AWSN.

The rest of this paper is organized as follows. Section II discusses the related work. Results from the link characterization experiments are detailed in Section III. Conclusion and future work is discussed in Section IV.

2 Related Work

There is a vast body of research work available in literature covering the link characterization for terrestrial WSN [6], [18], [19], [20] and [21] etc. These research studies found that low-power wireless links in WSN are susceptible to spatial as well as temporal variability. Authors in [6] proved that radio connectivity is not a simple disk while [19] and [20] showed the presence of "grey area" in wireless communications with high variance in packet reception rates. Zuniga et.al. in [21] described three distinct reception regions in a wireless link: connected, transitional, and disconnected. The transitional region has highly unreliable links and its region bounds can be found either by analytical or empirical methods [21] [8]. Our experimental study also confirmed the presence of grey zone of communications for 3D wireless sensor networks.

Studies covering link characterization for 3D wireless networks reported in the literature are based on different types of communication link technologies - (i) WiFi links [9], [10] (ii) a combination of WiFi and cellular communications [11], [12] (iii) ZigBee based links [13], [14], [15]. Authors in [13] showed that antenna orientation is a dominant factor affecting the RSSI sensitivity especially for 3D scenarios. Their empirical study was based on ZigBee based network using mon-pole antennas.

Allred et.al. in [14] presented results from their ZigBee based wireless characterization experiments using XBee Pro mounted SensorFlock platform. The quarter wave whip antenna used in their experiments also showed orientation bias. Teh et.al. [15] used the Fleck3 platform mounted on a fixed wing airborne vehicle to perform communication range testing. They employed an external antenna with the Fleck operating at 900 MHz band. In contrast, we employed a widely used ZigBee based TelosB platform, with embedded antenna, for our systematic link characterization experiments.

Estimation of the quality of wireless links is vital for optimizing protocols in wireless sensor networks. Srinivasan et.al. [22] showed that received signal strength indicator (RSSI) is a useful link quality indicator. He et.al. in [23] used RSSI to predict link quality for topology control through local optimization of nodes transmission power levels. We used RSSI in combination with packet reception rates as metrics to classify links in our characterization experiments.

3 Link Characterization Experiments

We conducted three sets of experiments employing the TelosB platform. The first set of experiments, referred as the antenna orientation experiments, aims to quantify the performance of the TelosB platform with respect to the node mounting position and the sender-receiver antenna orientation. The antenna on-board the TelosB is a standard inverted F type antenna and its typical radiation pattern is not truly omni-directional [17]. The mounting position of the WSN node on the UAV would thus affect the signal radiation in different directions. We assume that the WSN node is mounted in a fixed position (either horizontally or vertically) and that the antenna orientation can be changed dynamically with the rotation of the UAV. These experiments were performed with the A-G setting, with sender at a height above ground while the receivers located close to the ground. The second set of experiments evaluate three different kind of communications links namely G-A, A-A and A-G with respect to varying distances and heights above ground. This set is called the single-hop experiment. The last set of experiments, called the multi-hop experiment, evaluates the performance of the three different kinds of communications links simultaneously. This experiment captures the effect of inter-link interference in a multi-hop environment.

All of these experiments were conducted outdoors in a parkland (Centennial Parklands, Sydney). In order to measure the external interference caused by WiFi operating on the same 2.4 GHz frequency band, we first conducted a radio frequency spectrum survey using a spectrum analyzer and found only a single wireless access point occasionally active on WiFi channel 6. All WSN nodes were tuned to operate on ZigBee channel 26 known to be immune from the external interference. The floor noise level measured by the TelosB nodes vary between -90 to -93 dBm. The transmission power for all the nodes was set at 0 dBm (maximum power).

3.1 System Calibration

We first performed system calibration of the TelosB nodes to measure the node-to-node differences in the receiver sensitivities. We mounted SMA receptacle jacks on TelosB nodes (disabling the PCB inverted F antenna) and connected each node to a sender of known signal power through a 1.5m coaxial cable. This wired setup enabled us to measure each receiver response to a signal of known power from the sender. We observed that six of the eight tested TelosB exhibit similar receiver behavior and that response from only two nodes differ by +/- 2dB from the rest of the tested nodes. This calibration data was used to adjust the actual data collected in the characterization experiments. We also noticed poor PRR when the nodes were placed directly on the ground, while placing the nodes at 4cm above the ground on inverted foam glasses improved the performance. For the rest of this paper, ground placement actually refers to the node being placed just above the ground (4cm to be exact).

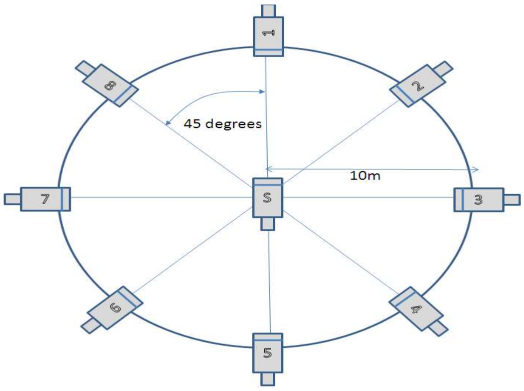

Figure 3.1: Topology for the Antenna Orientation Experiments

3.2 Antenna Orientation Experiments

We employed nine TelosB nodes for this experiment. One node was configured as the sender, programmed to send broadcast packets at the rate of 300 packets per minute (inter packet interval of 200 msec). Rest of the nodes received these broadcast packets and logged the sequence numbers and RSSI values in their flash. We arranged the nodes in a star topology with the sender at the center and receiver arranged at 45 degree angles at a distance of 10m from the center (Figure 3.1). Receivers were placed on the ground with their antenna facing towards the center. We varied the height of the sender node mounted horizontally on a plastic pole for different run of the experiments. Sender rotation was achieved by changing the direction of the sender 45 degrees after every three minutes. The experiment was then repeated with three different sender nodes to avoid any possible hardware bias. We ensured that minimum individual battery level was above 1.4V for all the experiments.

Figure 3.2 shows the result of sender antenna rotation experiment for one of the receiver node (Node No 6) with the sender height varied between 1.4m to 4.2m above ground. Zero degree rotation means that the sender and receiver antenna are directly facing each other. Results show that antenna

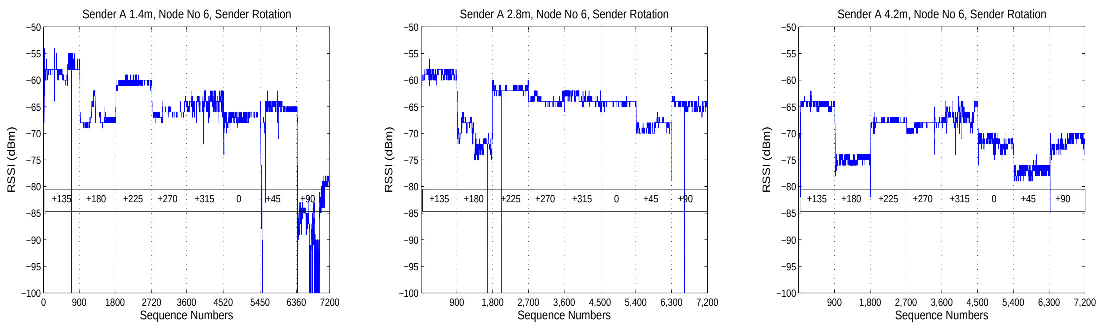

Figure 3.2: RSSI values with Sender Rotation for Varying Heights

orientation affects the RSSI values at the receiving nodes. We observed that on average RSSI values vary up to about 10dB for the best and worst antenna orientation for all height variations. Best RSSI values are always observed when the sender antenna is oriented at an angle of either 135 or 225 degrees with respect to the receiver antenna. This observation is consistent for all the receivers, for all height variations for the three different senders (for detailed results see Appendix A).

We used the average RSSI values received at all the eight receiver nodes to plot the radiation pattern for the three different sender nodes. Radiation pattern for sender A for height 2.8m is shown in Figure 3.3. Figure 3.3 shows that the radiation pattern is not truly omni-directional with higher values received in 135 and 225 degree sender antenna orientation with respect to the receiver antenna. Similar behavior was observed with sender placed at different heights.

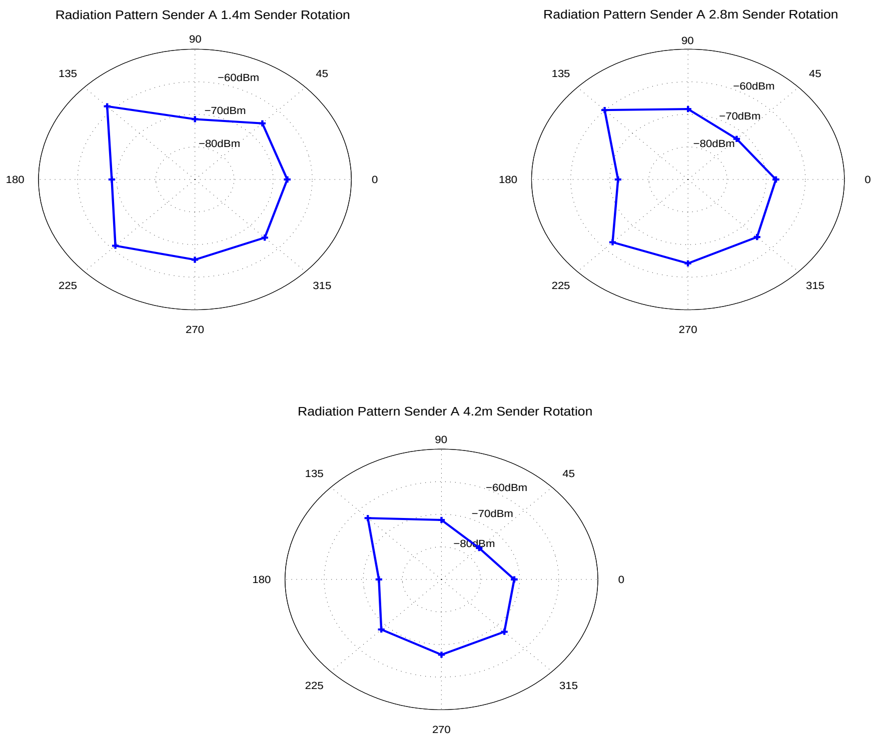

Figure 3.3: Radiation Pattern for TelosB Sender

We next conducted another granular experiment, where eight receivers were placed at 10 degree orientation around the sender and the sender was rotated by 45 degrees to cover the full 360 degrees rotation, in order to plot the fine-grained radiation pattern for the TelosB nodes. The radiation pattern observed is shown in Figure 3.4, where average RSSI values across all the receiver nodes have been plotted. The results show the existence of regions of better RSSI reception at around 135 and 225 degree orientation. Figure 3.5 shows the location of these regions of better RSSI reception by taking average across all the three senders. This confirms that the radiation pattern is not truly omni-directional and that the RSSI values depend on the relative direction of the receiver in the sender's antenna radiation pattern.

Note that the RSSI values are affected by a variety of factors beside the antenna orientation. In

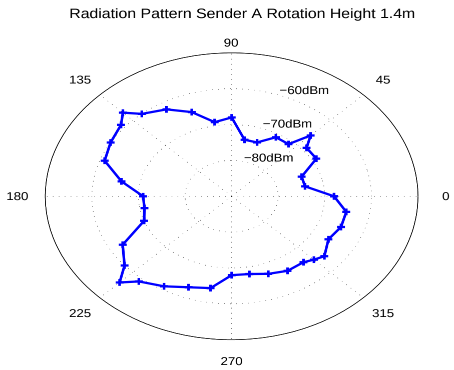

Figure 3.4: Radiation Pattern for a TelosB Sender

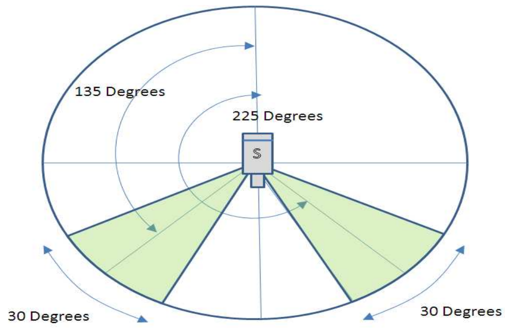

Figure 3.5: Regions of better RSSI radiation for TelosB

order to isolate the experimental results from the effect of fading and multi-path, we conducted an experiment in a RF anechoic chamber to plot nodes' free-space antenna patterns. Both sender and the receivers were placed about 1m above the ground. RSSI values at receivers were also confirmed by a co-located spectrum analyzer (model Anritsu 2721A) for the sender rotation in the anechoic chamber (for details refer to Appendix A.4). The spectrum analyzer has a 2.4 GHz external antenna as compared to the inverted-F antenna onboard the TelosB nodes. The radiation pattern observed in the anechoic chamber shown in Figure No 3.6, confirms the dependence of RSSI on antenna orientation similar to the one observed in the outdoor experiments.

We also conducted a variation of the sender rotation experiment where the sender is vertically mounted on the plastic pipe and rotated along the vertical axis (see Appendix A.5). Comparing Figure 3.7 with Figure 3.2 for node 6, we observe that horizontal mounting results in much better RSSI values than the vertical mounting. This implies that AWN nodes should have horizontally mounted TelosB nodes for improved performance.

We next conducted another set of experiments to investigate the effect of receiver antenna orientation on the RSSI values. Our objective was to find out whether the RSSI values can be further improved by changing the receiver antenna orientation while the sender antenna was at constant orientation with respect to the receiver. We conducted experiments with different sender antenna orientation with the same star topology but with 45 degree receiver rotation taking place after every

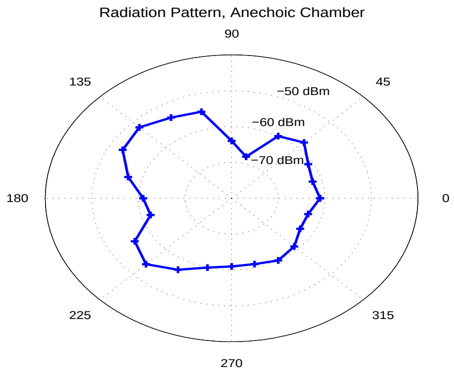

Figure 3.6: Radiation Pattern in RF-Anechoic Chamber

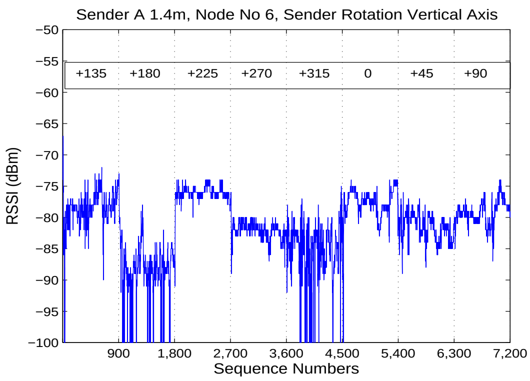

Figure 3.7: RSSI values for Vertically Mounted Sender Rotation

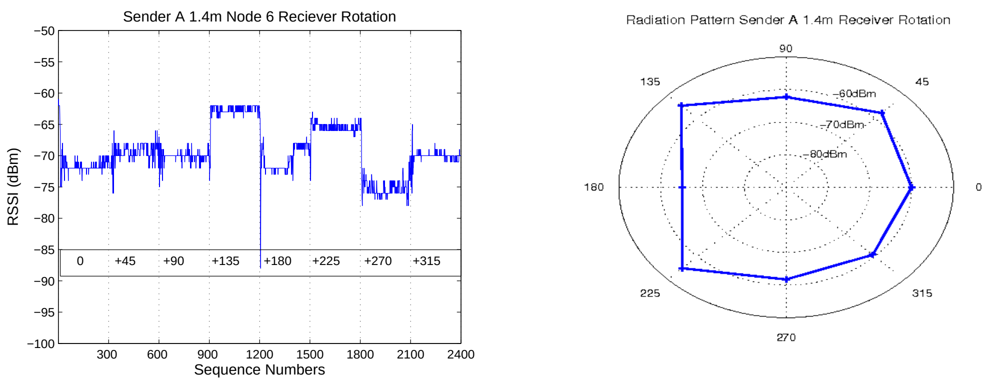

Figure 3.8: RSSI Values for Receiver Rotation and the Radiation Pattern

minute. The sender is also rotated by 45 degrees after every eight minutes such that it made a constant angle with the corresponding rotating receiver (see Appendix A.6).

The results in Figure 3.8 is for sender antenna orientation of 135 degree. Results show that RSSI values increases by about 6dB when the receiver antenna is oriented at 135 degrees with respect to the constant sender orientation. The experiment was repeated for different constant sender orientations with best results obtained when both sender's and receiver's preferred regions of RSSI overlap each other as shown in Figure 3.9.

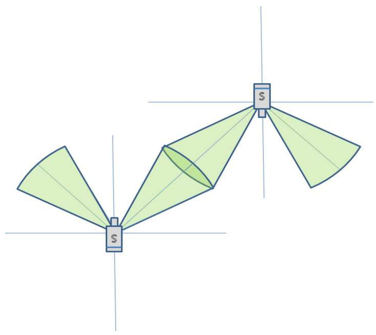

Figure 3.9: Best Sender and Receiver Orientations

In summary, following are the key findings from the first set of experiments:

1. The TelosB devices exhibit directional bias in the observed radiation pattern with two distinct regions of better RSSI reception. This observation is useful for an aerial network where the UAV can rotate and orient itself to achieve much better network performance.

2. Horizontal mounting of the TelosB nodes on the UAV results in much improved RSSI values as compared with the vertical mounting.

3.3 Single-Hop Experiments

The objective of this experiment was to analyze the behavior of three different types of communication links that is G-A, A-A and A-G. We conducted these experiments with two TelosB motes communicating with each other. The sender node sends 300 data packets per minute to the receiver node, and the receiver replies back to the sender. Both nodes log the RSSI and sequence numbers of each received packet. We measured the RSSI and the packet reception rates (PRR) for different sender/receiver height combinations (0.04m, 1.4m, 2.8m and 4.2m) and by increasing the distance between the nodes in increment of 10m until the PRR dropped below 20%. Antenna orientation for both sender and receiver was kept constant (parallel to each other and pointing in the same direction) for all run of these experiments.

Figure 3.10 shows the results for G-A case when the sender is placed at about 4cm above ground on an inverted foam glass for varying heights of the receiver. We observed that the RSSI and PRR improves when the height of the receiver is increased. Worst performance is achieved when both sender and receiver are close to the ground. Raising the receiver about 1.4m and 2.8m above ground results in successful PRR of greater than 80% for distances up to 40m and 70m respectively. The reason for performance improvement can be attributed to the effect of ground (reflections, absorptions etc) being reduced when the receiver is raised above the ground. Thus for G-A communications better reception rate is achieved for longer distances when the receiver is placed further up from the ground.

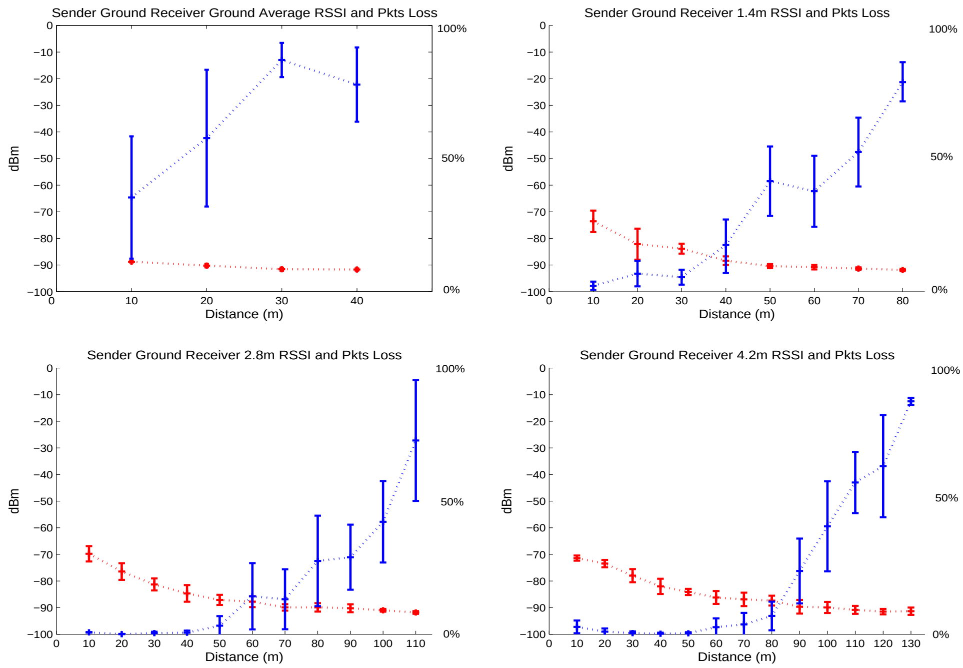

Figure 3.10: RSSI and Packet Loss Values for Ground to Air Communications

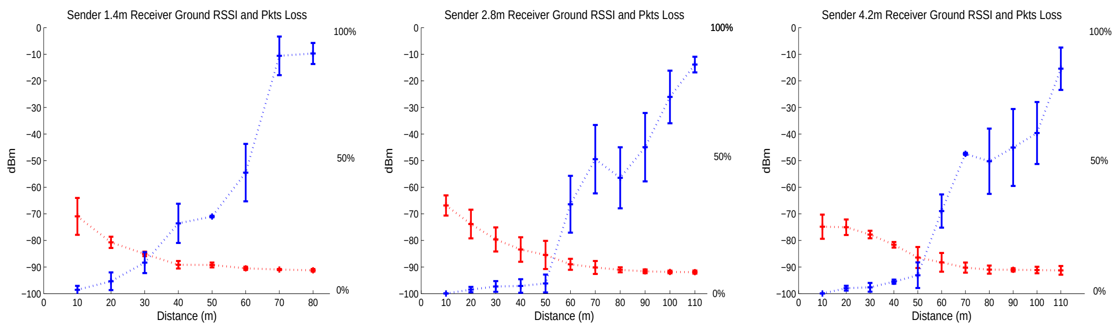

Figure 3.11: RSSI and Packet Loss Values for Air to Ground Communications

Figure 3.11 shows the results for Air-Ground communication (A-G) links when the height of the sender is increased from 1.4m to 2.8m and 4.2m above ground while the receiver is placed about 0.4cm above ground. We observed that generally successful packet reception rate improves with increase in height of the sender due to reduced effect of ground. Comparing the results for G-A and A-G communications in Figures 3.10 and 3.11, we found that G-A communications links perform better than the A-G links where better packet reception rates are obtained at longer distances. Several factors can contribute to this difference in performance between A-G and G-A links. For example, change in location of receiver in the sender's antenna radiation pattern for A-G and G-A communications (Section No 3.2), shadowing effect caused by blocking of line-of-sight by node's hardware [10] and variation in the ground reflections.

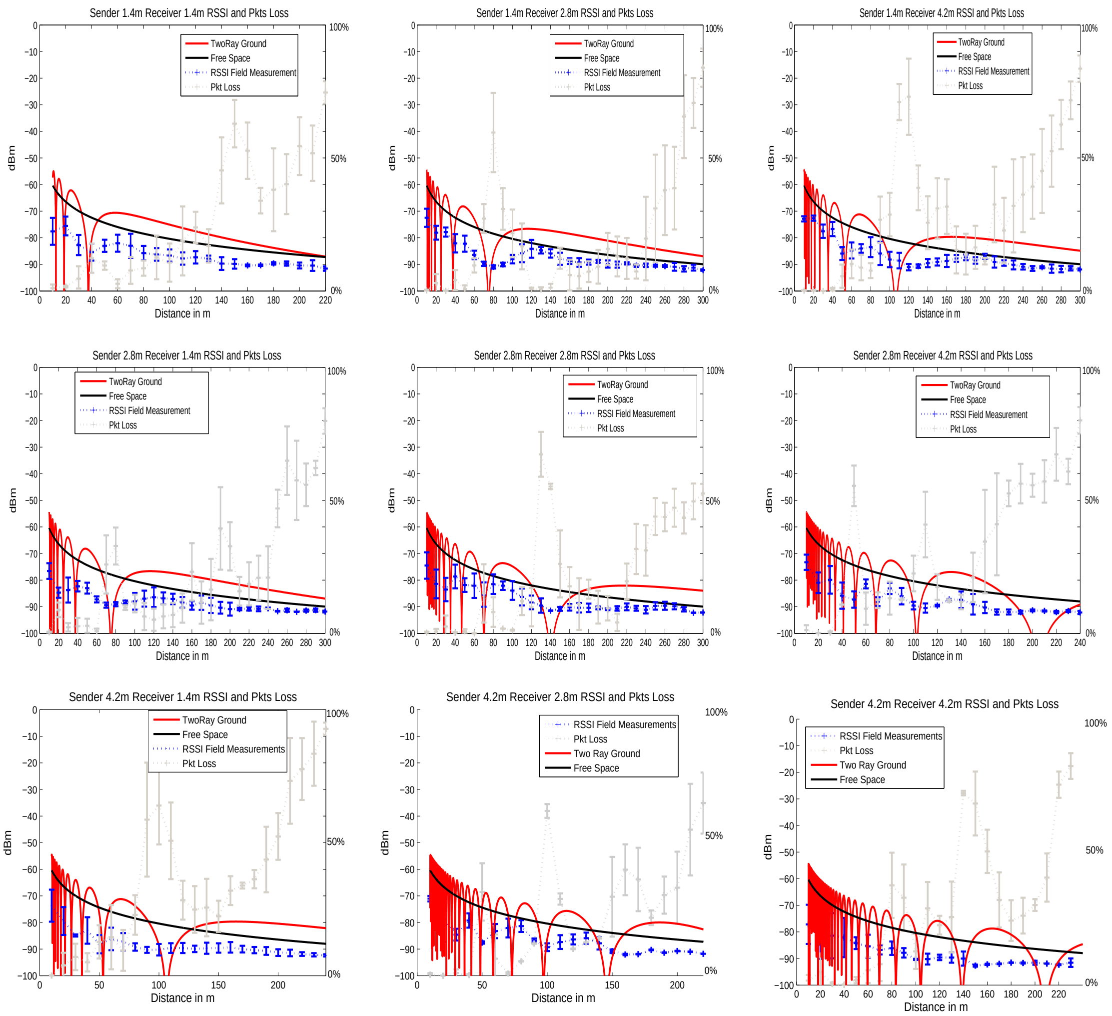

Figure 3.12: RSSI and Packet Loss Values for Air to Air Communication

We next conducted experiments to evaluate the performance of A-A communications links. Results are shown in Figure 3.12 where the expected path-loss given by Friis free space model and Two Ray Ground approximation model are also plotted. We note that as compared to the G-A and A-G scenarios, much better packet reception rates are obtained when both the sender and the receiver are at a height above the ground. Figure 3.12 shows that greater than 80% of successful packet reception rate is achieved up to a distance of 130m between the sender and receiver when both are at a height of 1.4m above the ground. The distance increases to about 220-240m when the sender is at 1.4m height and the receiver height is either 2.8m or 4.2m. We also observed the presence of grey regions of communication, where the PRR falls considerably before improving again when the receiver moves further away from the sender. The location of these grey zones depends both on the height of sender and the receiver e.g., for sender at 1.4m and receiver at 2.8m, it occurs at a distance around 80m from the sender.

Discussion

For better understanding of the grey regions, we re-visit the Friis free space and the Two Ray Ground approximation propagation models [26]. The free space model assumes no signal absorption or reflection in the environment. The transmit antenna is modelled as a point source with propagated energy spread over the surface of a spherical wavefront. If P_t is the transmit power, the power received P_r at a distance d is inversely proportional to the sphere surface area $4\pi d^2$ and is given by

$$P_r = \frac{P_t G_t G_r \lambda^2}{(4\pi d)^2} \tag{3.1}$$

where λ is the wavelength (speed of light divided by the carrier frequency) and G_t and G_r are the transmit and receive antenna gains respectively.

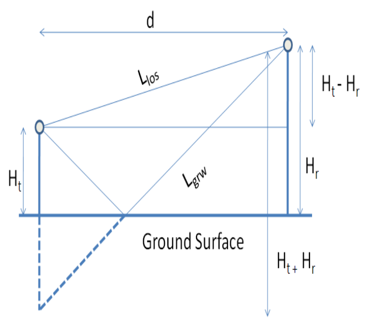

Figure 3.13: Two Ray Ground Model

The terrestrial propagation environment is not free space. Consider a pair of sender and receiver both at different heights above the ground as shown in Figure 3.13. If H_t represent the height of the sender antenna above ground and H_r the height for the receiver, then the length of the line of sight path (L_{los}) between the sender and receiver is given by

$$L_{los} = \sqrt{d^2 + (H_t - H_r)^2} \tag{3.2}$$

while the length of the ground reflected wave (L_{grw}) is given by Equation 3.3

$$L_{grw} = \sqrt{d^2 + (H_t + H_r)^2} \tag{3.3}$$

For a given distance d between the sender and receiver, the phase difference or shift between the two waves is then given by

$$\varphi = \frac{(L_{grw} - L_{los})2\pi}{\lambda} \tag{3.4}$$

We can thus calculate the distance between the sender and receiver, given the carrier frequency and the height of the sender and receiver, at which the phase shift is exactly π. At this distance the line of sight wave and the ground reflected wave tend to cancel each other out resulting in areas of poor reception as experienced in the field measurements. The Two Ray Ground approximation is given by

$$P_r = \frac{P_t G_t G_r \lambda^2}{(4\pi d)^2}\left[4sin\frac{\pi H_t H_r}{\lambda d}\right]^2 \tag{3.5}$$

Depending on the phase difference between the arriving signals, the interference can be either constructive or destructive, causing a very large observed difference in the amplitude of the received signal over very short distances. In our test environment, there were no obstruction nearby. So fading is pre-dominantly caused by ground reflections causing destructive interference to the original signal due to the multi-path fading effect. Comparing the expected path-loss given by Friis model (free space) and Two Ray Ground model in Figure 3.12, we can observe that the presence of grey zones coinciding with the points where Two Ray Ground model indicates presence of destructive interference. Note that the RSSI (and the packets loss) has been observed at discrete distances, in steps of 10m, which often does not exactly coincide with the continuous crest/troughs given by the theoretical Two Ray ground model approximation. Also note that the observed RSSI values are always lower than that given by the approximation models. This difference can be attributed to the assumptions made in the approximation model regarding the isotropic antenna behavior (we have already observed directional bias in Section 3.2) and ground reflection coefficient that affects the phase shift characteristics.

In summary, the experiments discussed in this section have highlighted the following important observations:

1. The Air-to-Air communications links perform the best among all types of links for the single-hop experiments.

2. The Ground-to-Air link performs better than the Air-to-Ground link when the ground nodes are placed at 4cm above ground.

3. The performance improves considerably when the sender/receiver are placed above the ground compared to the case when placed on the ground. For our experiments, a height of 1.4m gives much better result than placing the sender/receiver on the ground. This suggests that the base station should be placed at a height above the ground to achieve better PRR.

4. Grey zones are present when both the sender and receiver are placed at a height above the ground. This information is vital for resilient design of protocols in aerial WSN. The protocol designer must be aware of the presence of the grey zones due to fading and must incorporate remedial measure to alleviate the effect of such grey zones.

3.4 Multi-Hop Experiments

In the previous section, we measured the performance for three different kinds of links separately. We next conducted multi-hop experiments where all three types of links were used simultaneously. The objective was to measure the overall network performance in the presence of inter-link interference and to identify the bottleneck link for a multi-hop AWN.

The network topology is shown in Figure 3.14. The sender Node (Node 0) sends 1800 packets at the rate of 300 packets per minute addressed to Node 30 which replies back with Acks. All communication between Node 0 and 30 takes place over multi-hop links. Node 10 and 20 are the forwarding nodes in the topology. Node 0 and 30 are placed 4cm above ground while the height for the forwarding nodes is varied for different run of the experiment. All experiments were run with fixed antenna orientation for all the nodes.

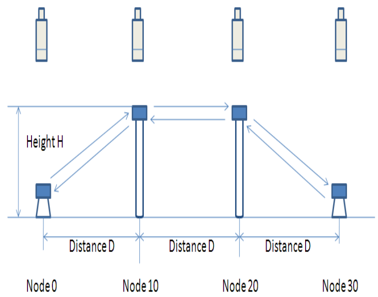

Figure 3.14: Topology for multi hop experiments, D and H varies. Top part shows antenna orientation for the nodes

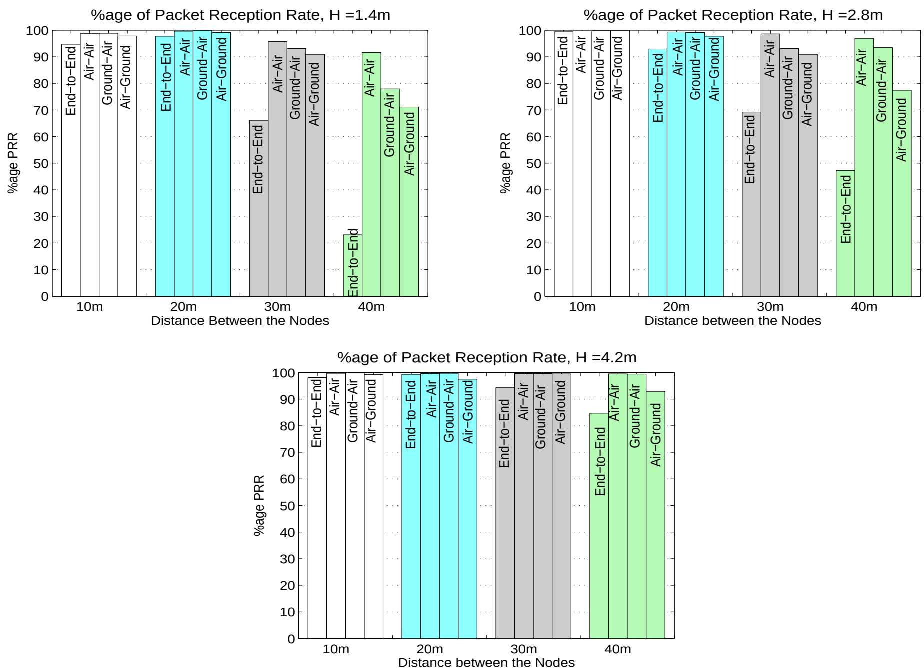

Figure 3.15: Packet Loss Values For Different Links

Figure 3.15 shows the overall PRR as well as the performance of different links for the multi-hop setup. The reported values are the average of the two multi-hop links, in forward (Node 0 to Node 30) and backward (Node 30 to Node 0) directions. The End-to-End PRR thus involves six communications links, two of each type A-G, A-A, and G-A. We can observe that for a fixed height (H) of the two forwarding nodes (Nodes 10 and 20), as expected, the End-to-End PRR deteriorates with the increase in the distance (D). The individual A-A links performed the best in multi-hop experiments while the A-G shows the worst performance. These results are consistent with the results from the single-hop experiments. Comparing the results for different heights for the forwarding nodes, the End-to-End PRR improves to about 48% when the forwarding nodes are raised to 2.8m above ground and to about 82% for 4.2m height of the forwarding nodes.

4 Conclusion and Future Work

We have presented results from an experimental study to characterize the link performance for an AWSN. The study highlighted that for TelosB platform antenna orientation and multi-path fading due to ground reflections affects the aerial link performance considerably.

We have observed that the TelosB PCB mounted inverted F antenna is not completely omni-directional (in 3D). As a future work, we will be investigating the use of externally mounted antennas to minimize losses and distortions in UAVs communications. Moreover, for UAVs that can keep a stable antenna orientation and travel more or less in the same plane, a single antenna might suffice, but in general a minimum of two, and probably more, antennas would be required for reliable communication in arbitrary directions between nodes of a distributed AWSN. We plan to investigate the use of dynamically switchable multiple antennas in AWSN that could be suitably arranged to cover communications in all directions. We have recently acquired MikroKopter HexaKopters [27] that we will utilize for our future aerial network experiments in a real 3D environment.

Bibliography

[1] K. Dantu, M. Rahimi, S. Babel, A. Dhariwal and G. Sukhatme, Robomote: Enabling Mobility in Sensor Networks, 2005: In Proceedings of IPSN/SPOTS 2005.

[2] I. Vasilescu, K. Kotay, D. Rus, Krill: An Exploration in Underwater Sensor Networks, 2005: In Proceedings of the Second IEEE Workshop on Embedded Networked Sensors (EmNetS-II).

[3] W.T.L. Teacy, J.Nie, S. McClean and G. Parr "Maintaining Connectivity in UAV Swarm Sensing", 2010:Proceedings of IEEE Globecom 2010 Workshop Wi-UAV, pages 1771-1776.

[4] S. Waharte N. Trigoni and S. J. Julier "Coordinated Search with a Swarm of UAVs", 2009: Proceedings of Sixth IEEE SECON 2009.

[5] N. Goddemeier, K. Daniel and C. Wietfield "Coverage Evaluation of Wireless Network of Unmanned Aerial Systems", 2010: Proceedings of IEEE Globecom 2010 Workshop Wi-UAV, pages 1760-1765.

[6] D. Ganesan, D. Estrin, A. Woo, and D. Culler, "Complex Behavior at Scale: An Experimental Study of Low-Power Wireless Sensor Networks", 2002, UCLA Computer Science Department UCLA/CSD-TR-02-0013.

[7] D. Kotz, C. Newport, and C. Elliot, "The Mistaken Axioms of Wireless Networks Research", 2003, Dartmouth College Computer Science TR-2003-467.

[8] K. Srinivasan, P. Dutta, A. Tavakoli, and P. Levis, "An Empirical Study of Low-power Wireless", 2010: ACM TOSN, pages 1-49.

[9] C. Cheng, P. Hsiao, H. Kung, and D. Vlah. "Performance Measurement of 802.11 a Wireless Links from UAV to Ground Nodes.", 2006: 15th International Conference on Computer Communications and Networks.

[10] D. Hague, H. T. Kung, and B. Suter. "Field Experimentation of COTS-based UAV Networking", 2006: IEEE MILCOM, Pages 1-7.

[11] K. Daniel, M. Putzke, B. Dusza, and C. Wietfeld, "Three Dimensional Channel Characterization for Low Altitude Aerial Vehicles",2010: Proceedings of International Symposium on Wireless Communication Systems ISWCS, pages 756-760.

[12] S. Rohde, N. Goddemeier, K. Daniel and C. Wietfield "Link Quality dependent Mobility Strategies for distributed Aerial sensor networks", 2010: Proceedings of IEEE Globecom 2010 Workshop Wi-UAV, pages 1783-1787.

[13] D. Lymberopoulus, Q. Lindsay, and A. Savvidas, "An Empirical Characterization of Radio Signal Strength Variability in 3-D IEEE 802.15.4 Networks Using Monopole Antennas", 2006: IEEE EWSN, LNCS 3860, pages 326-341.

[14] J. Allred, A. B. Hassan, S. Panichsakul, W. Pisane, P. Gray, J. Houang, R. Han, D. Lawrence, and K. Mohseni "SensorFlock: An Airborne Wireless Sensor Network of Micro-Air Vehicle",2007: Proceedings of SenSys2007, pages 117-129.

[15] S. Teh, L. Mejia, P. Corke, and W. Hu. "Experiments in Integrating Autonomous Uninhabited Aerial Vehicles (UAVs) and Wireless Sensor Networks.", 2008 Proceedings of The 2008 Australasian Conference on Robotics and Automation (ACRA 08).

[16] "Memsic Products", Available at http://www.memsic.com Accessed July 2011.

[17] "Datasheet for ChipCon Inverted F Antenna", Available at http://focus.ti.com/docs/prod/folders/print/cc2420.html Accessed July 2011.

[18] D. Lal, A. Manjeshwar, and F. Hermann. "Measurement and Characterization of Link Quality Metrics in Energy Constrained Wireless Senor Networks", 2003, Proceedings of The IEEE Globecom.

[19] A. Woo, T.Tong and D. Culler. "Taming the Underlying Challenges of Reliable Multi-Hop Routing in Sensor Networks" 2003, SenSys'03.

[20] J.Zhao and R. Govindan. "Understanding Packet Delivery Performance in Dense Wireless Sensor Networks", 2003, SenSys'03.

[21] M. Zuniga and B. Krishnamachari, "Analyzing the Transitional Region in Low Power Wireless Links", 1st IEEE Conference on Sensor and Ad Hoc Communications and Networks (SECON '04).

[22] K. Srinivasan and P. Levis, RSSI is Under Appreciated, 2006, in EmNets'06.

[23] L. He, B. Yu and J. Xu "LQATC: Link Quality Assured Topology Control Algorithm in Sensor Networks" 2010, Wireless Communications Networking and Mobile Computing (WiCOM).

[24] M. Bahramgiri, M. Hajiaghayi, V. S. Mirrokni "Fault-tolerent and 3-Dimensional Distributed Topology Control Algorithms in Wireless Muti-hop Networks" 2006, Wireless Networks. 12(2):pages 392-397.

[25] A. Ghosh, Y. Wang, B. Krishnamachari "Efficient Distributed Topology Control in 3-Dimensional Wireless Networks." 2007, Sensor, Mesh and Ad Hoc Communications and Networks, 2007. SECON '07. pages 91-100.

[26] T. S. Rappaport, "Wireless Communications : Principles and Practice", 1996, Prentice Hall New Jersey.

[27] "MikroKopter Hexa2 HexaKopter", Available at http://www.mikrokopter.de/ucwiki/en/MK-Hexa Accessed July 2011.

A Orientation Experiments

In this section, we list antenna orientation experiment results for all the eight nodes for three different heights with three different sender nodes A, B and C.

A.1 Sender A, Sender Rotation

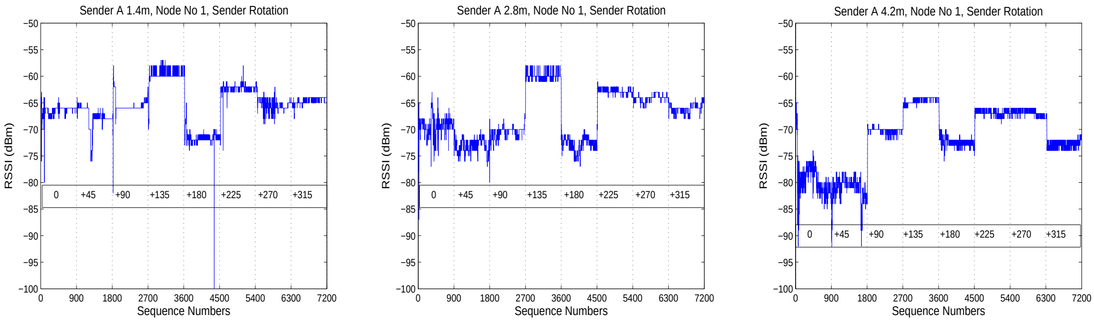

Figure A.1: RSSI values for Node 1 with Sender A Rotation for Varying Heights

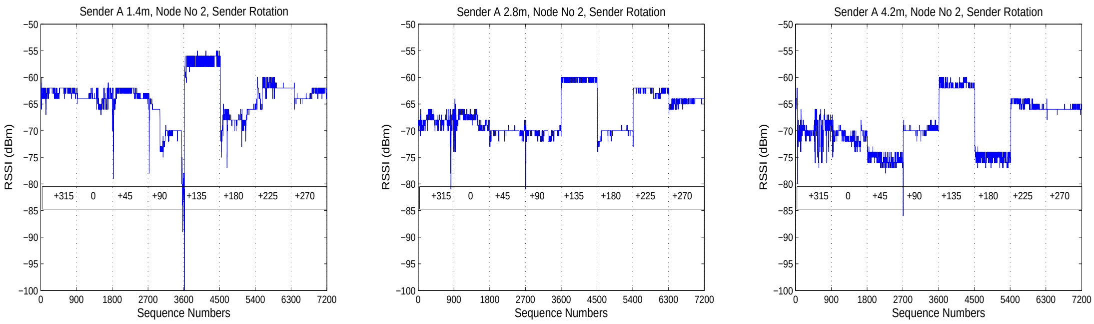

Figure A.2: RSSI values for Node 2 with Sender A Rotation for Varying Heights

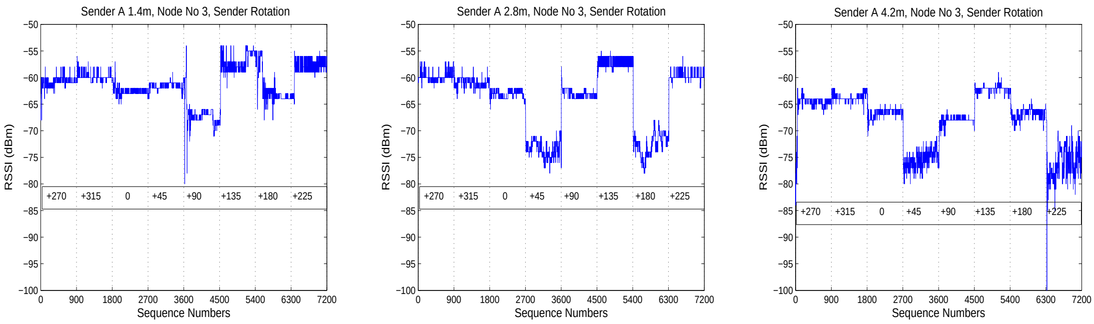

Figure A.3: RSSI values for Node 3 with Sender A Rotation for Varying Heights

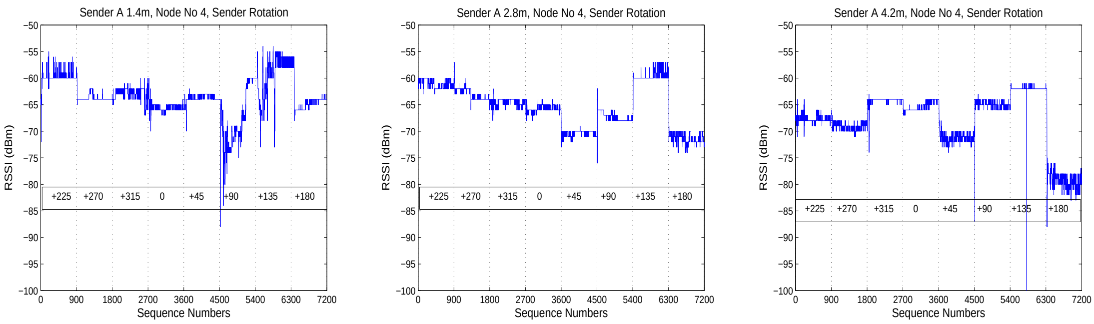

Figure A.4: RSSI values for Node 4 with Sender A Rotation for Varying Heights

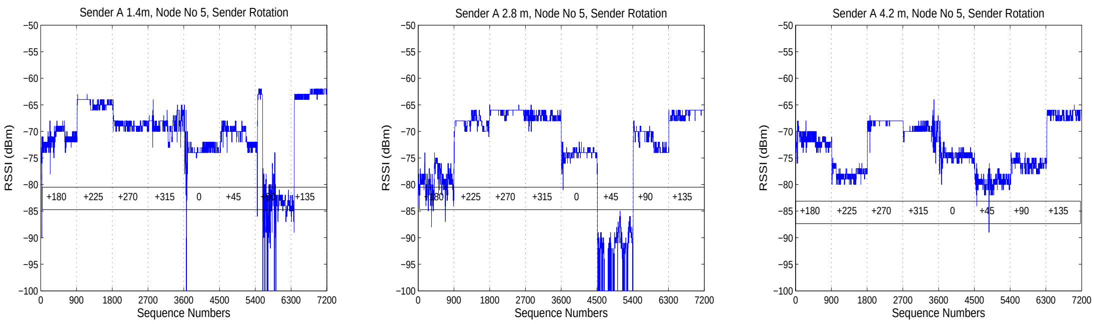

Figure A.5: RSSI values for Node 5 with Sender A Rotation for Varying Heights

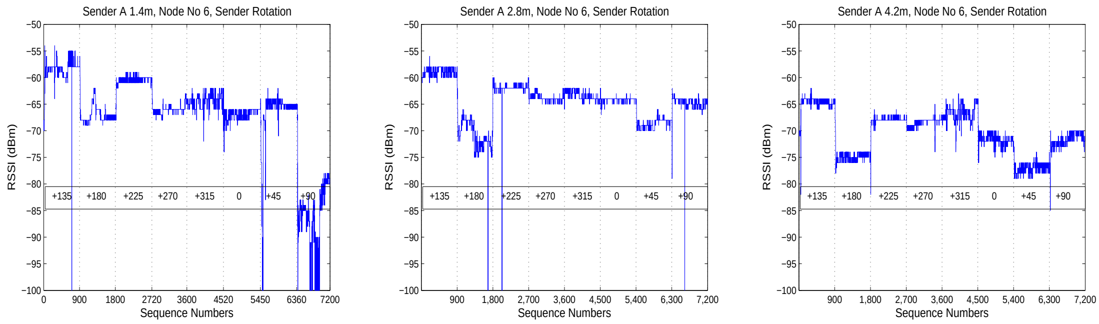

Figure A.6: RSSI values for Node 6 with Sender A Rotation for Varying Heights

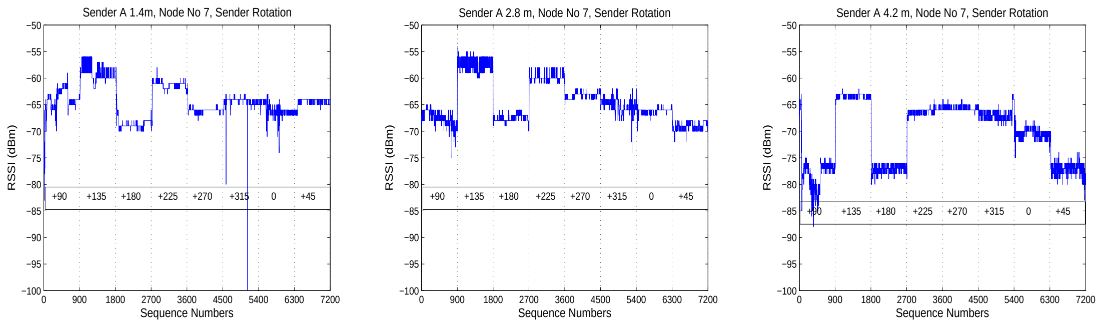

Figure A.7: RSSI values for Node 7 with Sender A Rotation for Varying Heights

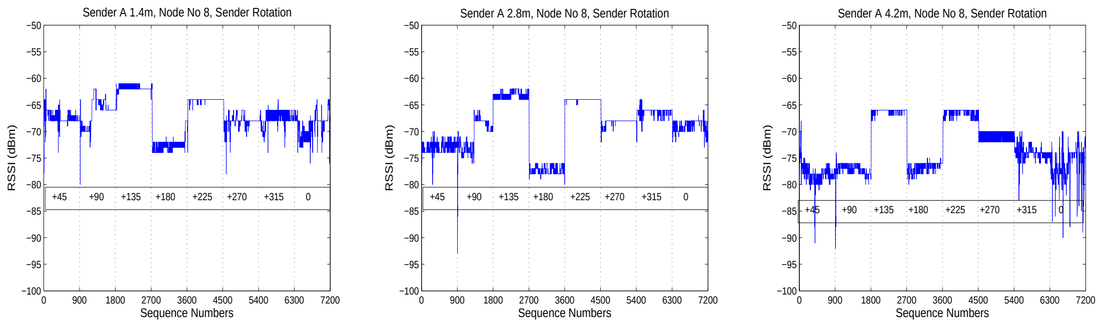

Figure A.8: RSSI values for Node 8 with Sender A Rotation for Varying Heights

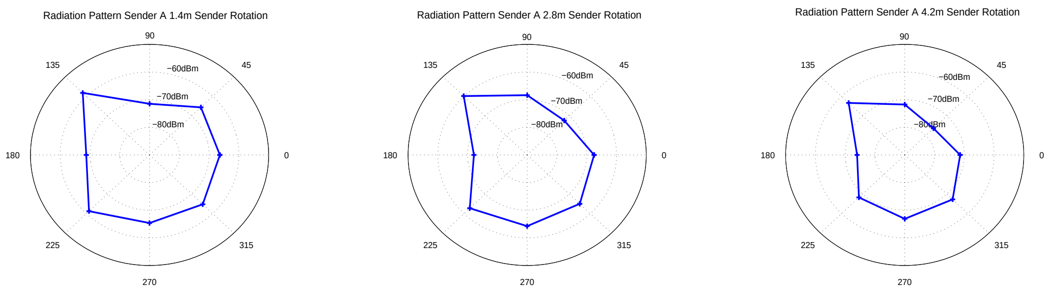

Figure A.9: Observed Radiation Pattern for Sender A Rotation for Varying Heights

A.2 Sender B, Sender Rotation

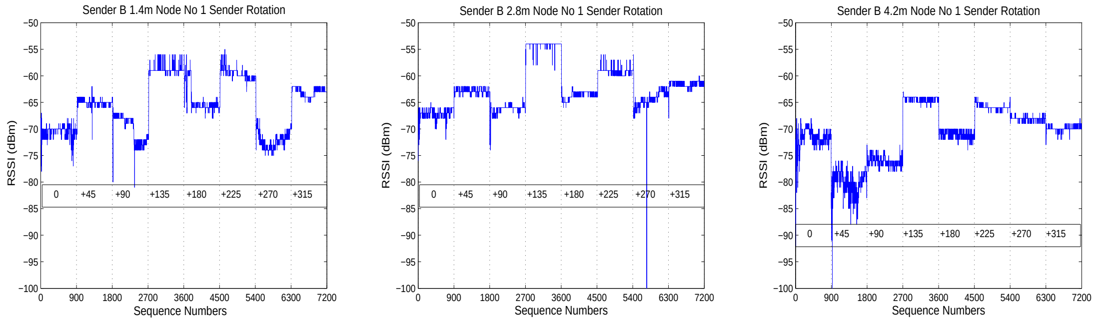

Figure A.10: RSSI values for Node 1 with Sender B Rotation for Varying Heights

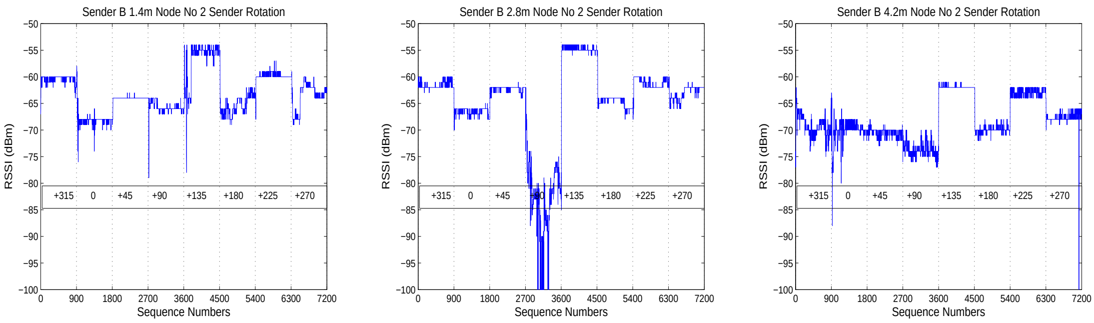

Figure A.11: RSSI values for Node 2 with Sender B Rotation for Varying Heights

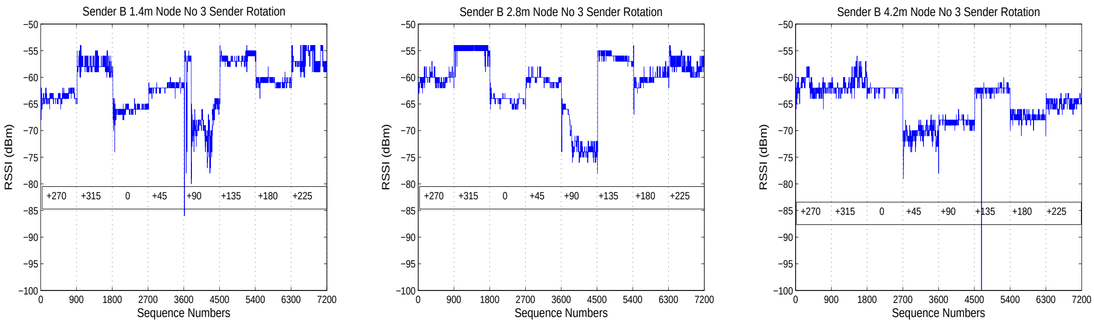

Figure A.12: RSSI values for Node 3 with Sender B Rotation for Varying Heights

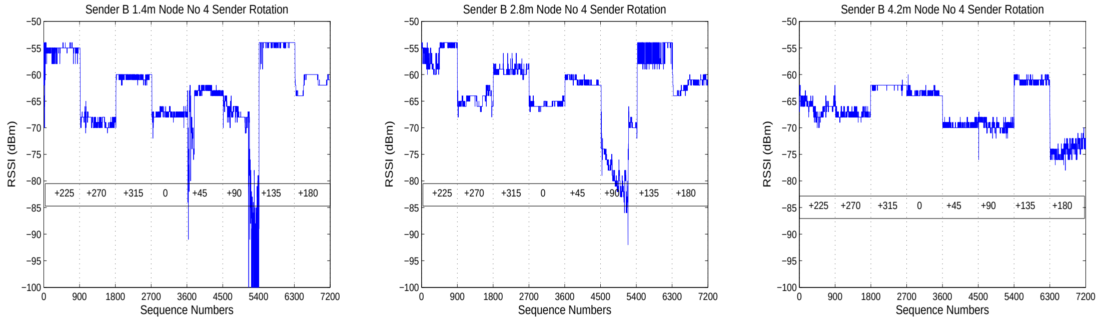

Figure A.13: RSSI values for Node 4 with Sender B Rotation for Varying Heights

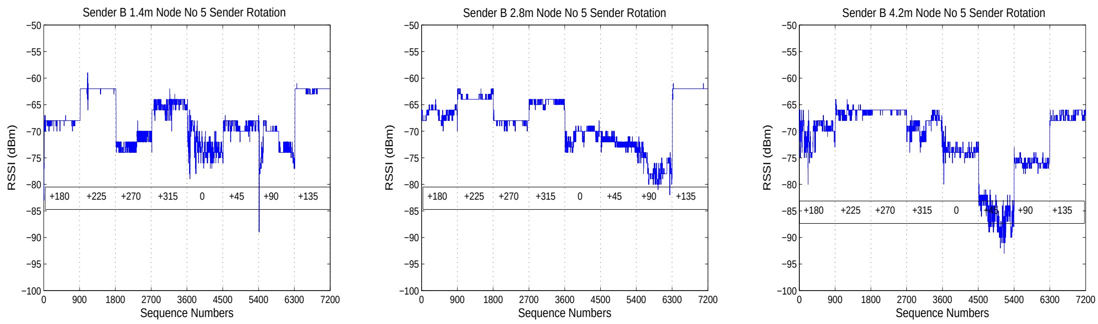

Figure A.14: RSSI values for Node 5 with Sender B Rotation for Varying Heights

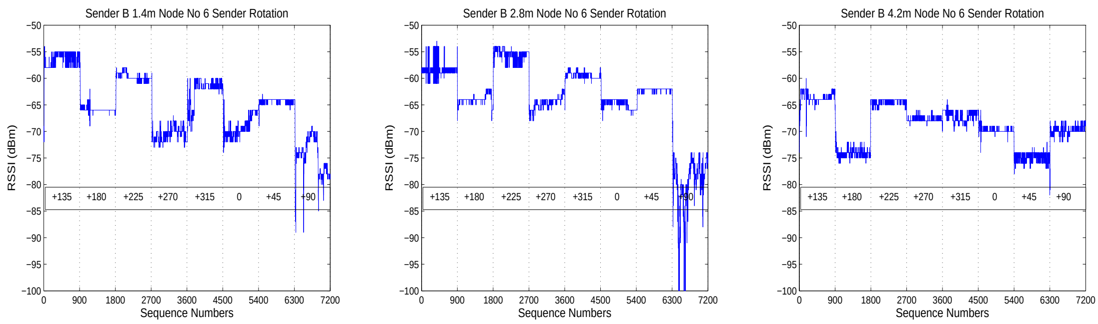

Figure A.15: RSSI values for Node 6 with Sender B Rotation for Varying Heights

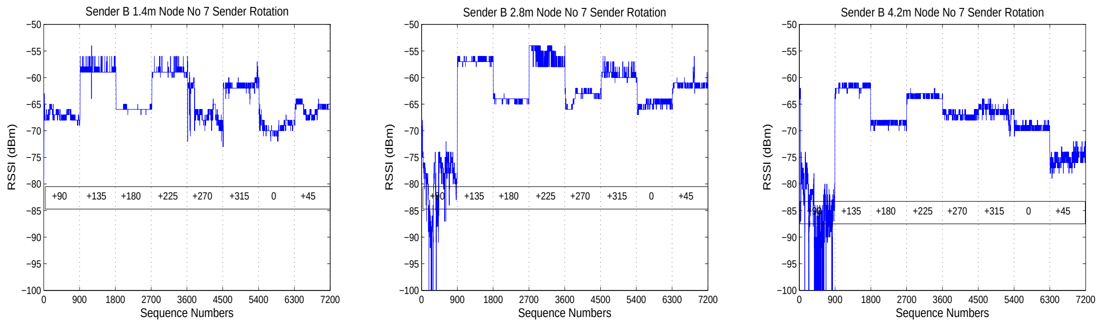

Figure A.16: RSSI values for Node 7 with Sender B Rotation for Varying Heights

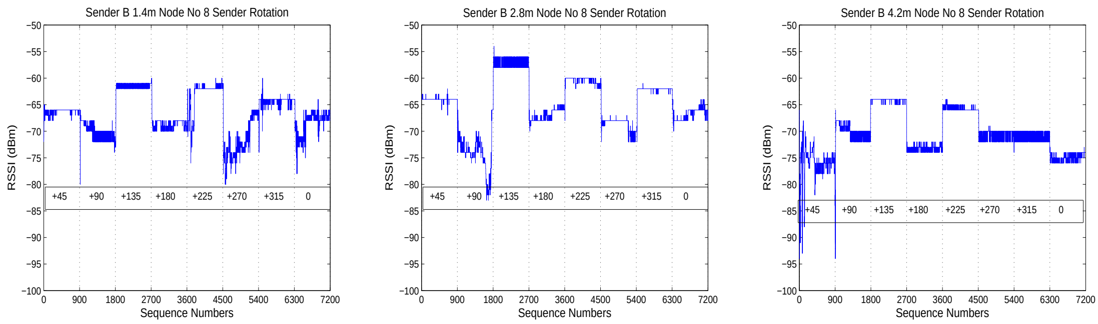

Figure A.17: RSSI values for Node 8 with Sender B Rotation for Varying Heights

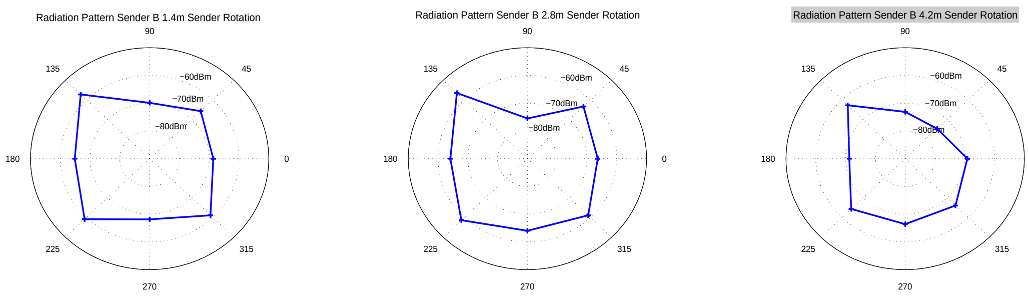

Figure A.18: Observed Radiation Pattern for Sender B Rotation for Varying Heights

A.3 Sender C, Sender Rotation

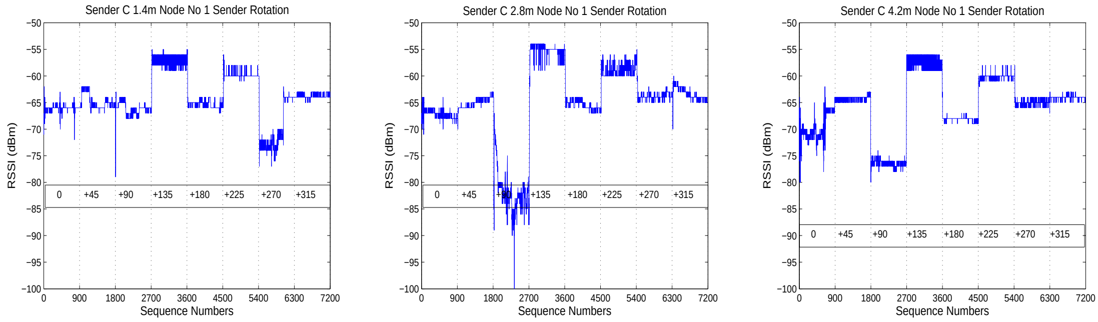

Figure A.19: RSSI values for Node 1 with Sender C Rotation for Varying Heights

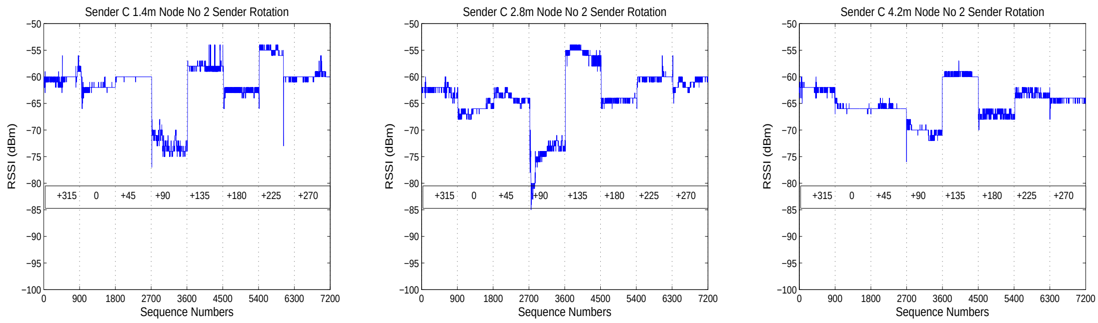

Figure A.20: RSSI values for Node 2 with Sender C Rotation for Varying Heights

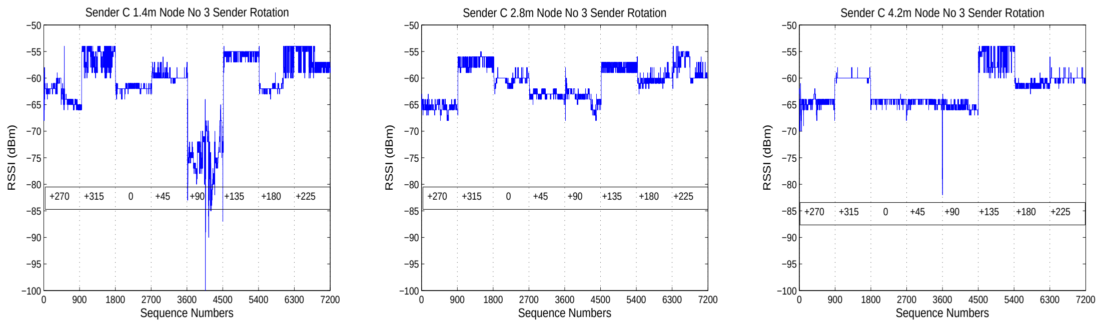

Figure A.21: RSSI values for Node 3 with Sender C Rotation for Varying Heights

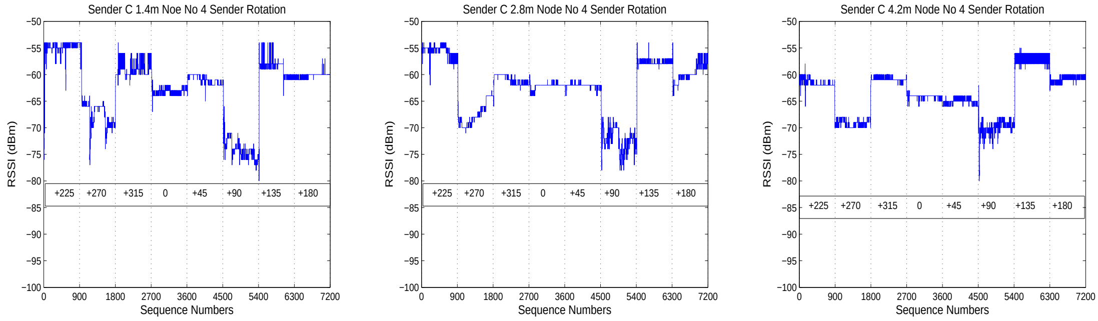

Figure A.22: RSSI values for Node 4 with Sender C Rotation for Varying Heights

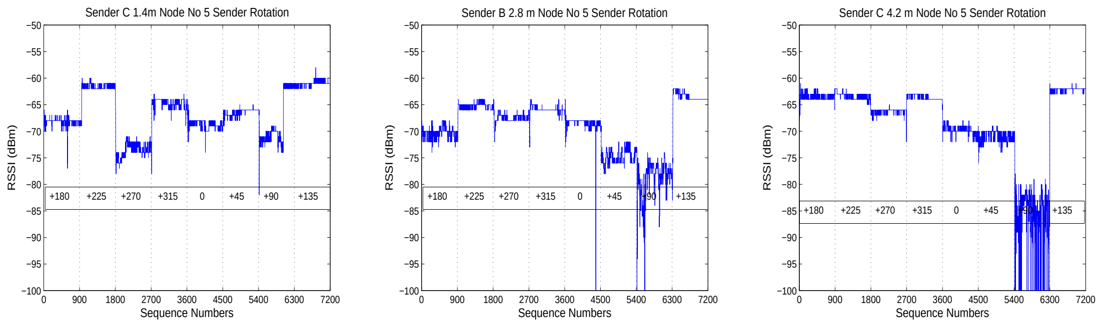

Figure A.23: RSSI values for Node 5 with Sender C Rotation for Varying Heights

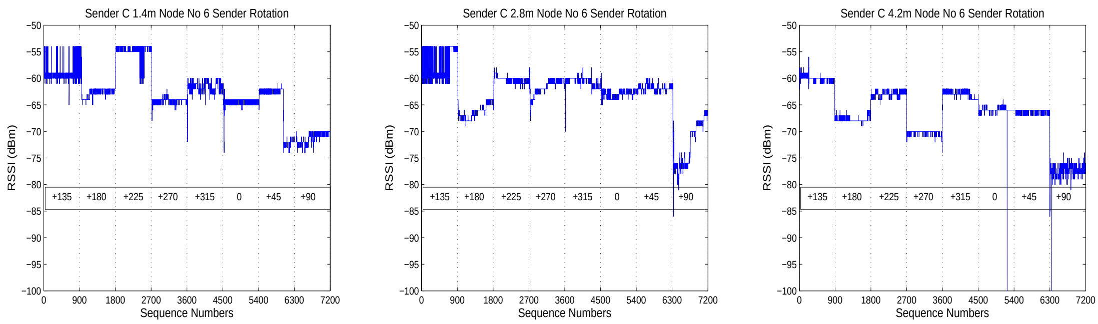

Figure A.24: RSSI values for Node 6 with Sender C Rotation for Varying Heights

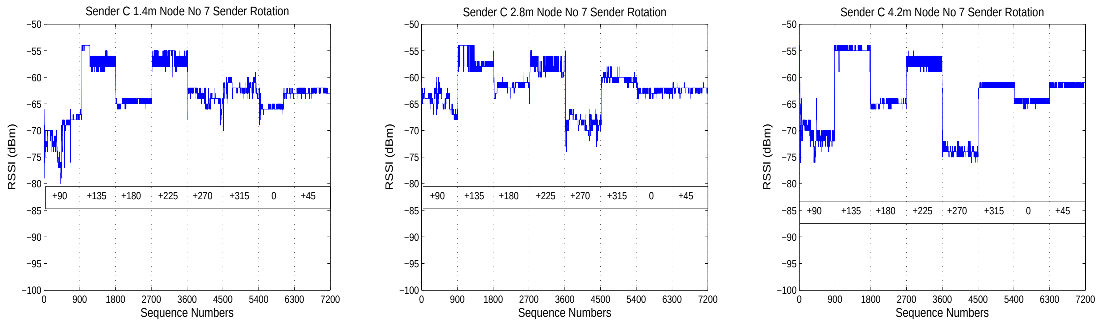

Figure A.25: RSSI values for Node 7 with Sender C Rotation for Varying Heights

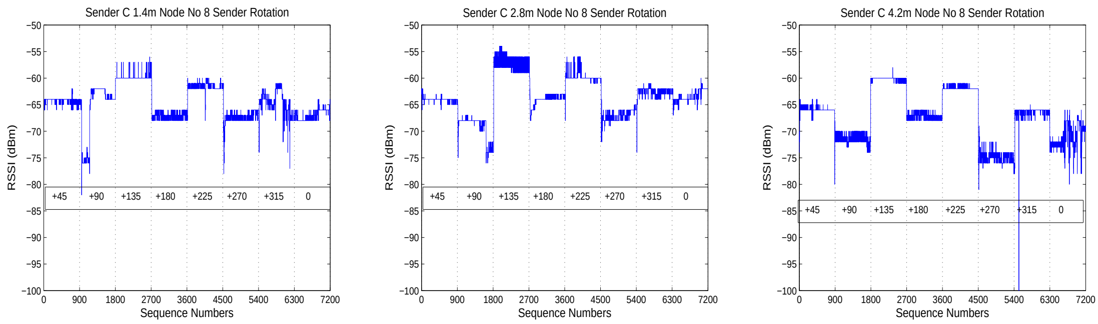

Figure A.26: RSSI values for Node 8 with Sender C Rotation for Varying Heights

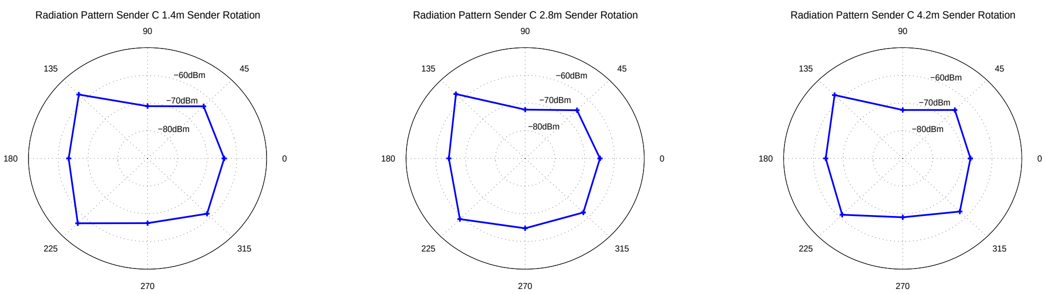

Figure A.27: Observed Radiation Pattern for Sender C Rotation for Varying Heights

A.4 Sender A, Sender Rotation, RF Anechoic Chamber

In this section, we present the experimental results when the nodes are placed in an RF anechoic chamber. Both the sender and the receivers were placed about 1m above the ground.

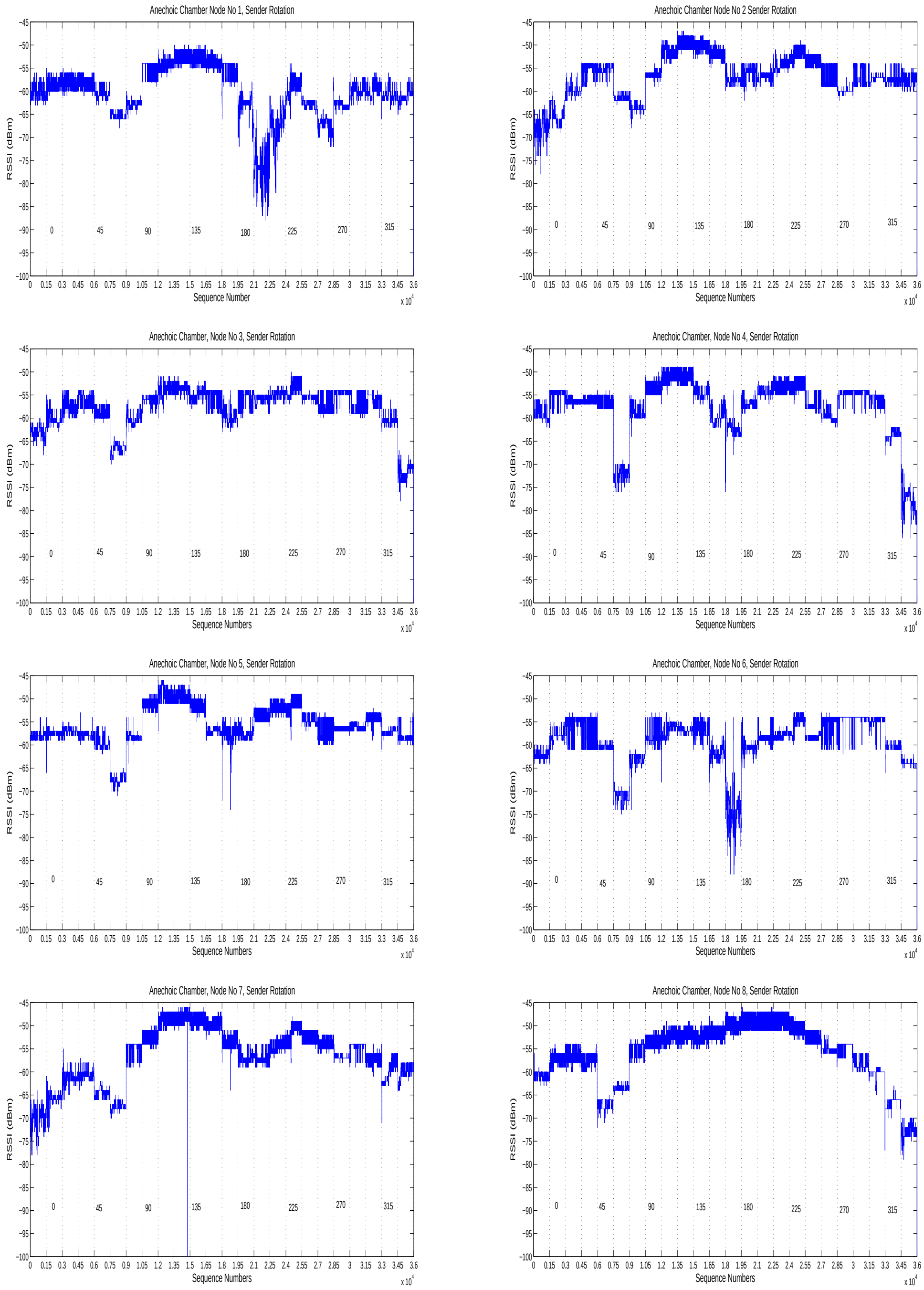

Figure A.28: RSSI values for Nodes with Sender A Rotation Anechoic Chamber

A.5 Sender A, Sender Rotation, Vertical Axis

This section shows characterization results when the sender is vertically mounted on a plastic pole and rotated along the vertical axis. Receivers were placed at the ground.

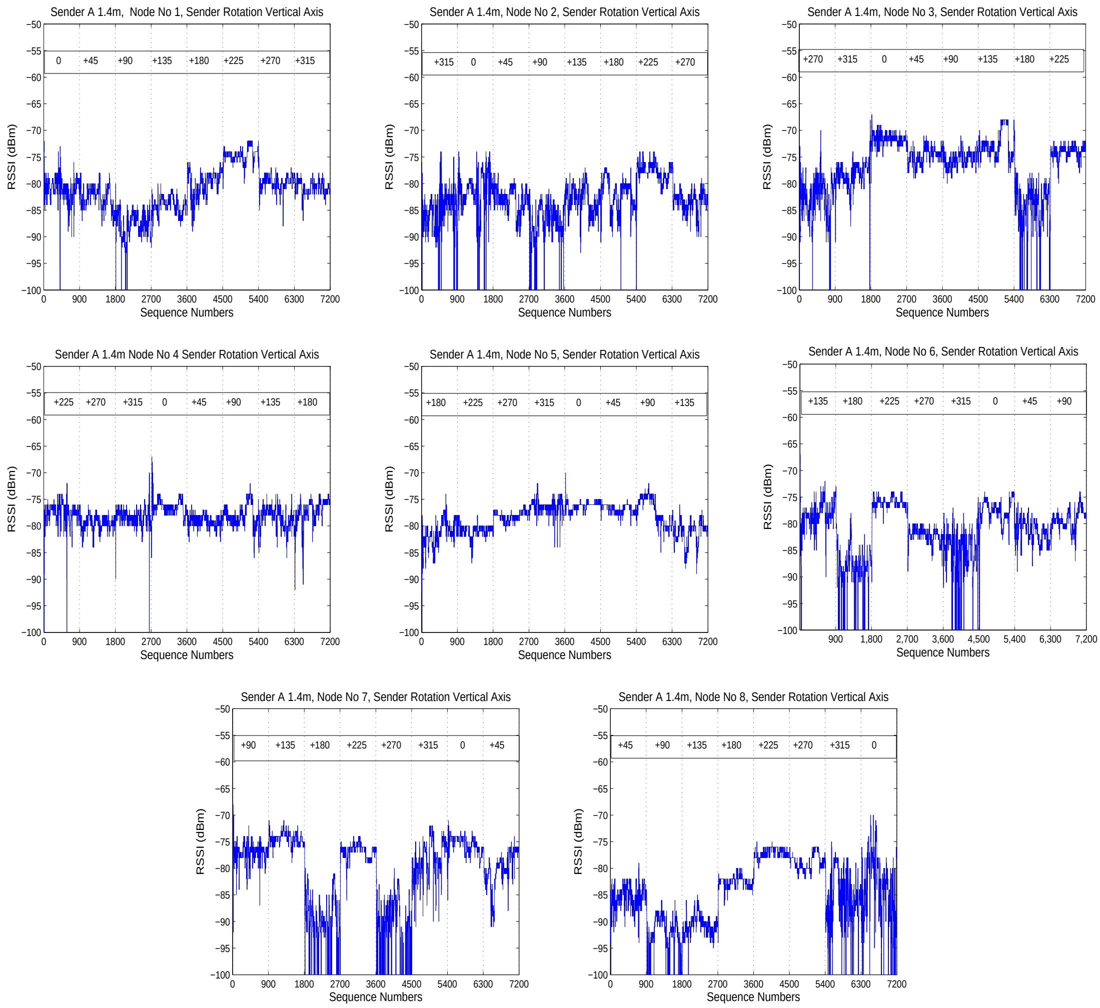

Figure A.29: RSSI values for Nodes with Sender A Rotation along Vertical Axis for Varying Heights

A.6 Sender A, Receiver Rotation

Link characterization results for receiver rotation for a constant sender orientation.

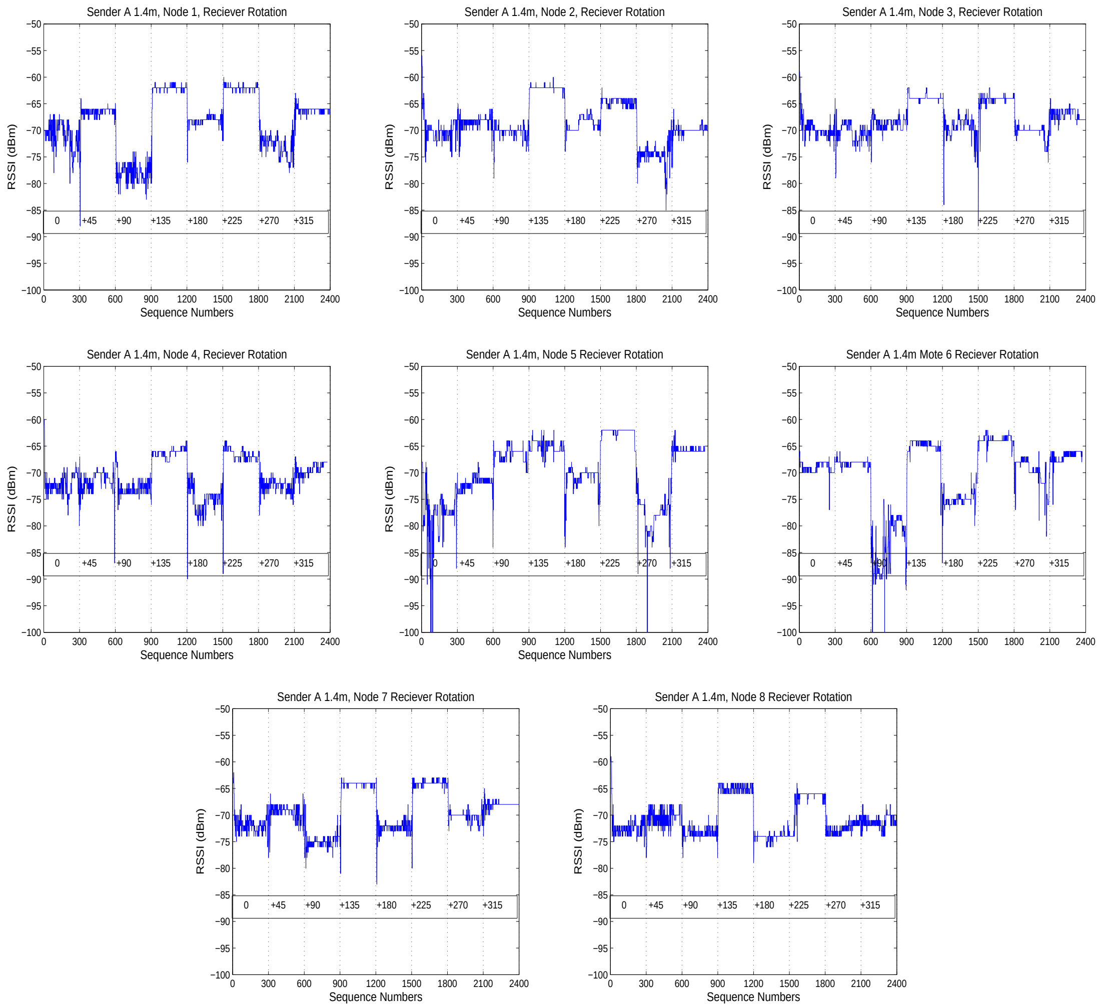

Figure A.30: RSSI values for Nodes with Sender A Receiver Rotation